Fully Printed Dual-Band Power Divider Miniaturized by CRLH Phase-Shift Lines

Da-jeong Eom and Sungtek Kahng

In this letter, a compact and fully printed composite right- and left-handed (CRLH) dual-band power divider is proposed. The branches of the conventional Wilkinson power divider are replaced by subwavelength CRLH phase-shift lines having +90˚ for one frequency and –90˚ for another frequency for dual-band and miniaturization performance. Equations are derived for the even- and odd-mode analysis combined with the dual-band CRLH circuit. A PCS and a WLAN band are chosen as the test case and the circuit approach agrees with the CAD simulation and the measurement. Additionally, the CRLH property is shown with the dispersion diagram and the eightfold size reduction is noted.

Keywords: Dual-band power divider, CRLH, phase shift.

I. Introduction

Power dividers are widely used in RF systems, such as array antennas, measurement equipment, and so on [1]. Numerous research and design approaches have been carried out to meet challenging requirements, such as multiband, multiport, and shorter power dividers [2], [3]. The conventional dual-band power divider used harmonics [4], lumped elements [5], [6], and a multisection branch line [7].

To overcome the limitation in size reduction, metamaterials have intrigued wireless communication system designers [8], [9]. Using the lumped elements of the composite right- and left-handed (CRLH) structure for the nonlinear dispersion curve, Caloz and Itoh provided the dual-band characteristics for a branch coupler and a four-port power divider [8]. The branches of the power divider are replaced with the

Table 1. Specifications of dual-band power divider.

Item	Specification for power divider
Band 1	0.8 GHz to 1.1 GHz
Band 2	2.2 GHz to 2.5 GHz
Return loss (S_{11})	≤ –15 dB
Outputs (S_{21}, S_{31})	≤ 3 ±1 dB
Isolation (S_{32})	≤ –15 dB

complementary split ring resonators under the signal lines by Marques and others to reduce the size [9].

We propose a compact dual-band power divider as fully printed nonlumped capacitance and inductance elements, such as distributed element transmission lines. The size of the entire structure is reduced by devising a CRLH phase-shift line to have 90º at one frequency and –90º at another. The circuit of the CRLH phase-shift line is obtained by the equations for the even- and odd-mode analysis incorporated with the CRLH configuration and realized with interdigital lines and short stubs, which make this component fully printed and capable of being integrated without lumped elements. To verify the proposed method, the specifications in Table 1 are given for the design.

The CRLH phase-shift line will show Φ_1=90˚ at f_1=0.9 GHz and Φ_2=–90˚ at f_2=2.4 GHz. It is embedded in a power divider whose result will agree with the CAD simulation. Additionally, the full-wave simulation and measurement agree. It is revealed that the miniaturization is enabled by the distributed-element CRLH phase-shifter of the length < λ_g/23.

II. Dual-Band CRLH Phase-Shift Line

To reduce the size of the power divider and give it a dual-

band effect, a CRLH phase-shift line can be considered for the branches of the Wilkinson power divider. This CRLH circuit should have the phases of 90° at f_1, and −90° at f_2. Firstly, the π-type equivalent circuit is set as Fig. 1.

In this particular design, the shunt capacitance (C_R), series capacitance (C_L), series inductance (L_R), and shunt inductance (L_L) are determined by generating 90° at f_1 and −90° at f_2 through the relationship between the phase and LC circuit [8], [10]. As a matter of course, the zeroth-order resonance (ZOR) should also be created around $(f_1+f_2)/2$ for the size reduction [10]. Therefore, the mathematical expressions for C_R, C_L, L_R, and L_L are as follows:

$$C_R = \frac{\pi[(\frac{\omega_1}{\omega_2}+1)]}{2\omega_2 Z_c[1-(\frac{\omega_1}{\omega_2})^2]}, \quad C_L = \frac{2\pi[(1-\frac{\omega_1}{\omega_2})]}{\omega_1 Z_c[1+(\frac{\omega_1}{\omega_2})^2]},$$

$$L_R = \frac{Z_c\pi[(\frac{\omega_1}{\omega_2}+1)]}{2\omega_2[1-(\frac{\omega_1}{\omega_2})^2]}, \quad L_L = \frac{2Z_c[(1-\frac{\omega_1}{\omega_2})]}{\pi\omega_1[1+(\frac{\omega_1}{\omega_2})^2]}, \quad (1)$$

where $\omega_1 = 2\pi f_1$, $\omega_2 = 2\pi f_2$, and Z_c in (1) is the output port impedance. Solving the equations by setting f_1 and f_2 at 0.9 GHz and 2.4 GHz, respectively, C_R, C_L, L_R, and L_L are 3.333 pF, 1.407 pF, 8.333 nH, and 3.518 nH, respectively. Using these elements, the phase is plotted with the dispersion diagram showing the CRLH and ZOR characteristics.
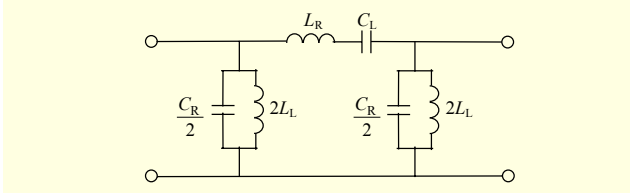

Fig. 1. Equivalent circuit of proposed dual-band CRLH phase-shift line.
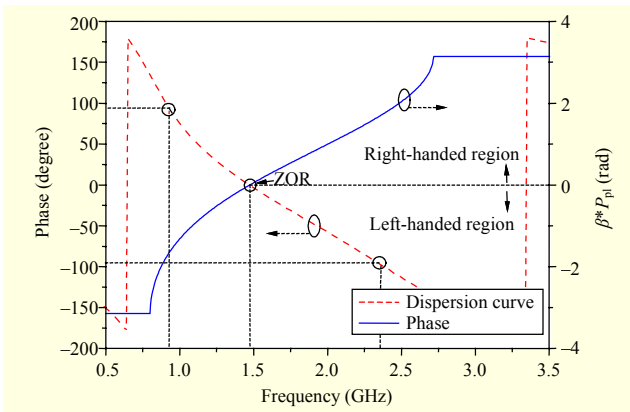

Fig. 2. Phase and dispersion of CRLH phase-shift line.

In Fig. 2, the phases of 90° and −90° are achieved at 0.9 GHz and 2.4 GHz, respectively, to be placed later for the power division. This phase-shift line complies with the specifications in Table 1 and will replace the 90° branches of the power divider for physical miniaturization. The dispersion curve in Fig. 2 shows the LH region ($\beta<0$) and the RH region ($\beta>0$), along with the ZOR near 1.47 GHz.

III. Even- and Odd-Mode Methods for Dual-Band CRLH Power Divider

For the purpose of making the power divider compact, the CRLH phase-shift line is placed in the branches from port 1 to ports 2 and 3. Since the power divider is symmetric, we can calculate the circuit elements and get S-parameters by using the even- and odd-mode analysis method.

As the power divider is designed, the closed form expression for the input impedance of the proposed CRLH phase-shift line is needed, because the power divider is combined with the CRLH circuit. To get Z-parameters, including the input impedance of the CRLH phase shifter, Fig. 1 is modified to become Fig. 3, where Y_{se} is the admittance of series L_R and C_L, and Y_{sh} is the admittance of shunt L_L and C_R.

Y_{se} and Y_{sh} are given as

$$Y_{se} = (j\omega L_R + \frac{1}{j\omega C_L})^{-1}, \quad Y_{sh} = \frac{j\omega C_R}{2} + \frac{1}{j\omega 2L_L}. \quad (2)$$

Based on the admittances above, the Z-parameters of the CRLH phase-shift line are derived as

$$Z_{11} = Z_{22} = \frac{Y_{se}^2 + Y_{se}Y_{sh}}{2Y_{se}^2 Y_{sh} + Y_{se}Y_{sh}^2}, \quad Z_{12} = Z_{21} = \frac{Y_{se}}{2Y_{se}Y_{sh} + Y_{sh}^2}. \quad (3)$$

With the Z-parameters of (3), Fig. 4 is generally treated as the schematic of Fig. 5. The input impedance of Figs. 4 and 5 is Z_{in}^{CRLH}. Thus, the input impedance in Fig. 4 can be manipulated as

$$Z_{in}^{CRLH} = \frac{V_1}{I_1} = Z_{11} - \frac{Z_{21}Z_{12}}{Z_L + Z_{22}}. \quad (4)$$

1. Even-Mode Case

The even-mode equivalent circuit is shown in Fig. 4(a). For the even-mode excitation, there is no current flow through the $R/2$ resistors. Therefore, the circuit element R is open-circuited.
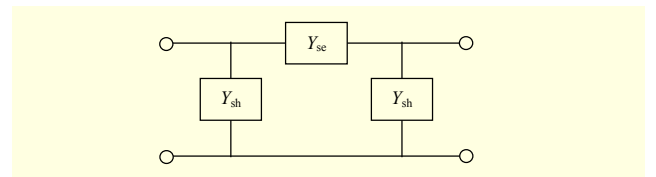

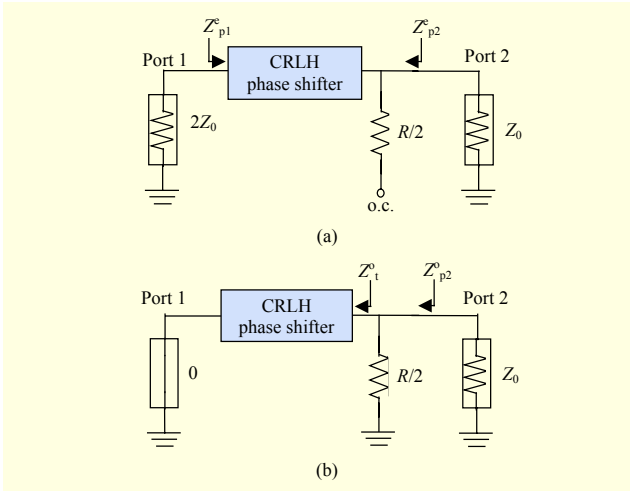Fig. 3. Admittance expression for CRLH phase shifter.

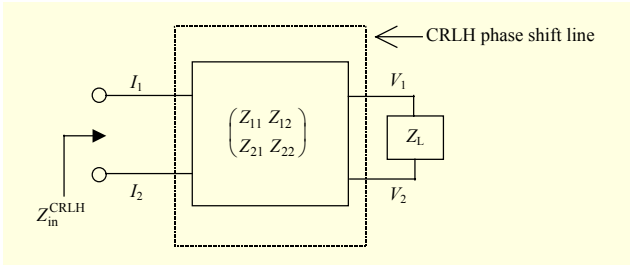Fig. 4. Proposed power divider: (a) even-mode model and (b) odd-mode model.

Fig. 5. Schematic for even-/odd-mode analysis with $Z_{\text{in}}^{\text{CRLH}}$.

Additionally, the impedance Z_0 at port 1 is doubled. To see S-parameters, we need the input impedance at port 1 (Z_{p1}^{e}) and the input impedance at port 2 (Z_{p2}^{e}). After mathematical procedures, Z_{p1}^{e} and Z_{p2}^{e} become

$$Z_{\text{p1}}^{\text{e}} = Z_{11} - \frac{Z_{12}Z_{21}}{Z_0 - Z_{22}}, \quad Z_{\text{p2}}^{\text{e}} = Z_{11} - \frac{Z_{12}Z_{21}}{2Z_0 + Z_{22}}. \quad (5)$$

2. Odd-Mode Case

Figure 4(b) is the odd-mode equivalent circuit. Here, we can assume there is an electric wall in the middle of ports 2 and 3. Port 1 is short circuited. Only the input impedance at port 2 is derived as

$$Z_{\text{p2}}^{\text{o}} = \left(\frac{1}{Z_{\text{t}}^{\text{o}}} + \frac{2}{R}\right)^{-1}, \quad (6)$$

where

$$Z_{\text{t}}^{\text{o}} = Z_{11} - \left(\frac{Z_{21}Z_{12}}{Z_{22}}\right). \quad (7)$$

R is obtained as 100 Ω, which plays the role of keeping the isolation between ports 2 and 3.

$$S_{11} = \frac{2Z_0 - Z_{\text{p1}}^{\text{e}}}{2Z_0 + Z_{\text{p1}}^{\text{e}}}, \quad S_{12} = S_{21} = \sqrt{\frac{1 - S_{11}^2}{2}},$$
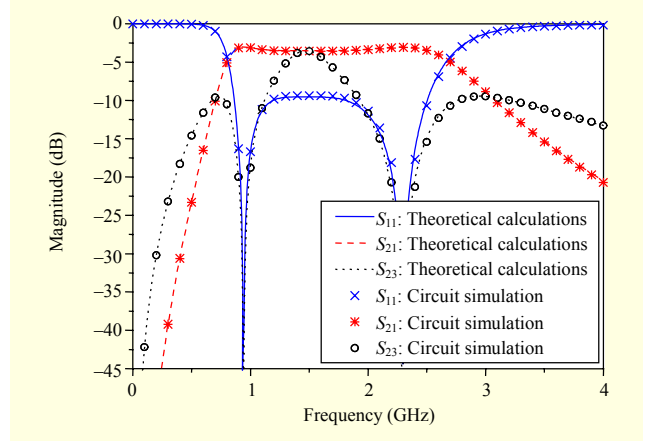

Fig. 6. Circuit simulated result of proposed power divider.

$$S_{22} = S_{33} = \frac{1}{2}\left(\frac{Z_{\text{p2}}^{\text{e}} - Z_0}{Z_{\text{p2}}^{\text{e}} + Z_0} + \frac{Z_{\text{p2}}^{\text{o}} - Z_0}{Z_{\text{p2}}^{\text{o}} + Z_0}\right),$$

$$S_{23} = \frac{1}{2}\left(\frac{Z_{\text{p2}}^{\text{e}} - Z_0}{Z_{\text{p2}}^{\text{e}} + Z_0} - \frac{Z_{\text{p2}}^{\text{o}} - Z_0}{Z_{\text{p2}}^{\text{o}} + Z_0}\right). \quad (8)$$

Using all the derived equations, we can observe the frequency response of the proposed power divider in terms of the equivalent circuit.

The S-parameters obtained by our equations are compared with those obtained by the Advanced Design System, and they agree, as shown in Fig. 6. The input power is equally divided to the output ports, since S_{21} and S_{31} are exactly the same. Also, the return loss is better than 15 dB and means excellent impedance matching over the dual band. Additionally, the isolation complies with the specifications.

IV. Fabrication and Measurement of Power Divider

The power divider is physically implemented. The geometrical shape for the full-wave simulation and the fabricated power divider are given in Fig. 7.

The physical dimensions shown in Fig. 7(a) are W=18.7, P_{p1}=7.7, $w1$=2.2, L=25, $l1$=3.4, $l2$=7.9, f_w=0.5, f_l=5.4, and f_g=0.2 (mm) with FR4 as the substrate and a 100-Ω chip resistor. A comparison of the measured and EM-simulated results is shown in Fig. 7(c). The total size is 18.7 mm×25 mm ×1.2 mm. The measurement in agreement with the simulation shows that S_{21} and S_{31}, S_{11}, and S_{32} are –3.5 dB, <–10 dB, and <–15 dB, respectively, at 0.9 GHz and 2.4 GHz in Fig. 7(c). Figure 7(d) shows that the phase difference between port 2 and port 3 is zero at the two bands. Table 2 reflects S_{21} and S_{31} at sample points of the two bands.

At the frequencies in each of the two bands, the values of S_{21} are similar to those at f_1 and f_2, since the curve changes slowly
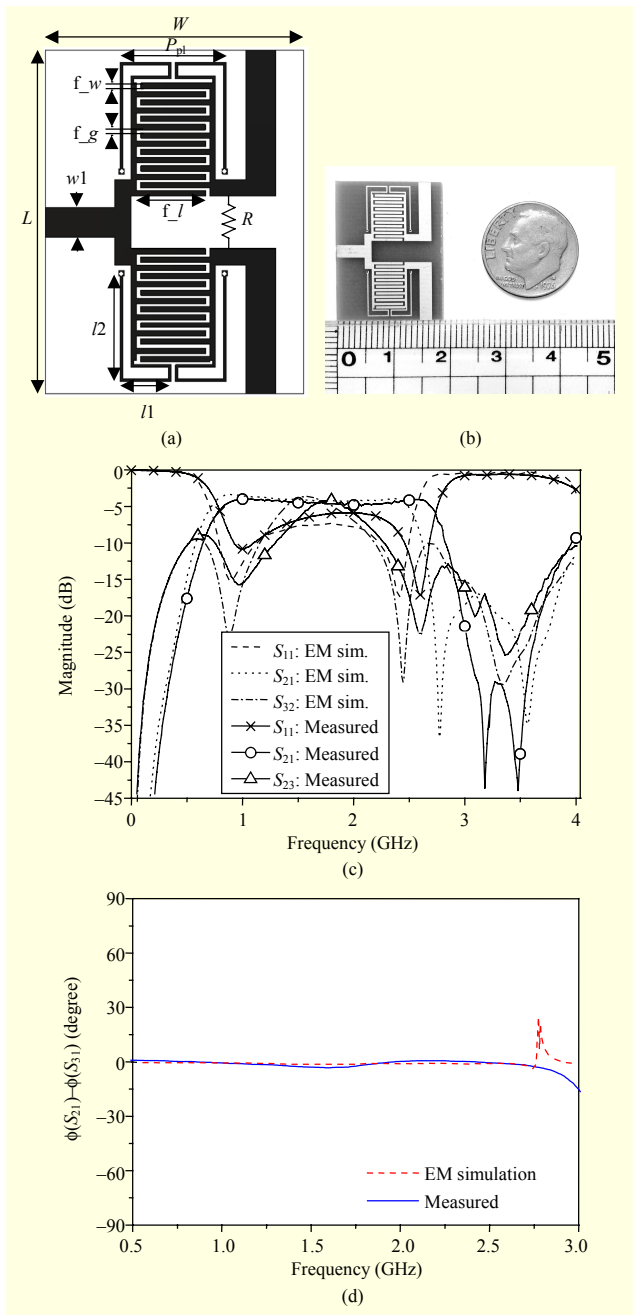
Fig. 7. Fabricated and EM-simulated proposed power divider: (a) geometry, (b) photo, (c) measurement vs. EM simulation, and (d) measured phase.

Table 2. S_{21} and S_{31} at sample frequencies in two bands.

Frequency (GHz)	0.8	0.9	1.1	2.2	2.4	2.5
S_{21}, S_{31} (dB)	−5.1	−3.6	−3.7	−4.7	−4.3	−4.1

over the bands. Additionally, it is thought that the proposed design can be adopted for dual-band antenna arrays with smaller footprints, as in [11].

V. Conclusion

A compact dual-band power divider was proposed. The branches of the conventional power divider were replaced by our CRLH phase shifter. Performances of S_{21} and S_{31} and those of S_{11} and S_{32} were obtained as −3.5 dB and −3.5 dB and < −15 dB and < −15 dB in the two target bands, respectively. The size was reduced by a factor of eight.

References

[1] D.M. Pozar, *Microwave Engineering*, 2nd ed. Hoboken, NJ: Wiley and Sons, Inc., 1998, pp. 367-368.

[2] H. Oraizi and A.-R. Sharifi, "Optimum Design of Asymmetrical Multisection Two-Way Power Dividers with Arbitraty Power Division and Impedance Matching," *IEEE Trans. Microw. Theory Tech.*, June 2011, pp. 1478-1490.

[3] I. Sakagami and T. Wuren, "Compact Multi-way Power Dividers for Dual-Band, Wide Band and Easy Fabrication," *IEEE Microw. Symp. Dig.*, Oct. 2009, pp.489-492.

[4] S. Srisathit et al., "A Dual-Band 3-dB Three-Port Power Divider Based on a Two-Section Transmission Line Transformer," *Proc. IEEE MTT-S Int. Microw. Symp. Dig.*, vol. 1, June 2003, pp. 35-38.

[5] L. Wu et al., "A Dual-Frequency Wilkinson Power Divider," *IEEE Trans. Microw. Theory Tech.*, vol. 54, no. 1, Jan. 2006, pp. 278-284.

[6] T. Kawai et al., "Dual-Band Wilkinson Power Dividers Using a Series RLC Circuit," *IEICE Trans.*, vol. E91-C, no. 11, Nov. 2008, pp. 1793-1797.

[7] D. Wang, W. Tang, and X. Xu, "Isolation Characteristics of Microstrip Wilkinson Dual-Band Power Divider," *Proc. Asia-Pacific Microw. Conf.*, Dec. 2008, Art. ID B1-02.

[8] C. Caloz and T. Itoh, *Electromagnetic Metamaterials: Transmission Line Theory and Microwave Application*, Hoboken, NJ: John Wiley & Sons, Inc., 2006.

[9] R. Marques, F. Martin, and M. Sorolla, *Metamaterials with Negative Parameters: Theory, Design, and Microwave Applications*, Hoboken, NJ: John Wiley and Sons, Inc., 2008, pp. 236-245.

[10] G. Jang and S. Kahng, "Compact Metamaterial Zeroth-Order Resonator Bandpass Filter for a UHF Band and Its Stopband Improvement by Transmission Zeros" *IET Microw., Antennas Propag.*, vol. 5, no. 10, 2011, pp. 1175-1181.

[11] J. Anguera et al., "Fractal-Shaped Antennas: A Review," *Wiley Encyclopedia of RF and Microwave Engineering*, K. Chang, Ed., vol. 2, 2005, pp. 1620-1635.